

**Excitation and detection of terahertz coherent spin waves in antiferromagnetic  $\alpha$ -Fe<sub>2</sub>O<sub>3</sub>**K. Grishunin<sup>Ⓧ,\*</sup>, E. A. Mashkovich<sup>Ⓧ,†</sup> and A. V. Kimel*Radboud University, Institute for Molecules and Materials, Nijmegen 6525AJ, Netherlands*A. M. Balbashov<sup>‡</sup>*Moscow Power Engineering Institute, Department of Physics of Electrical Materials and Components and Automation of Electric Technology Complexes, Moscow 111250, Russia*

A. K. Zvezdin

*Prokhorov General Physics Institute of the Russian Academy of Sciences, Theory Department, Moscow 119991, Russia*

(Received 8 March 2021; accepted 7 June 2021; published 14 July 2021)

The efficiency of the ultrafast excitation of spins in antiferromagnetic  $\alpha$ -Fe<sub>2</sub>O<sub>3</sub> using a nearly single-cycle THz pulse is studied as a function of the polarization of the THz pulse and the sample temperature. Above the Morin point the most efficient excitation is achieved when the magnetic field of the THz pulse is perpendicular to the antiferromagnetically coupled spins. Using the experimental results and equations of motion for spins, we show that the mechanism of the spin excitation above and below the Morin point relies on a magnetic-dipole interaction of the THz magnetic field with spins, and the mechanism implies that the efficiency of the coupling is proportional to the time derivative of the magnetic field.

DOI: [10.1103/PhysRevB.104.024419](https://doi.org/10.1103/PhysRevB.104.024419)**I. INTRODUCTION**

In quantum mechanics the interaction between two electrons depends on the mutual orientations of their spins. This short-range spin-dependent part of the electron-electron interaction, also known as the exchange interaction, is able to induce a long-range ferromagnetic and antiferromagnetic order of spins, respectively [1,2]. Although materials with ferromagnetic order (ferromagnets) are used in conventional magnetic data storage, spintronics, and magnonics technologies, antiferromagnets represent the largest, the least explored, and probably the most intriguing family of magnetically ordered materials in nature.

It is believed that antiferromagnets can dramatically improve the performance of these technologies in terms of densities and speed [3–5]. The absence of net magnetization and stray fields eliminates crosstalk between neighboring bits or devices [3], and the absence of primary macroscopic magnetization makes the spin manipulation in antiferromagnets inherently faster than in ferromagnets [4,6]. Fundamental studies of spin dynamics, the developments of means and approaches for the manipulation and detection of spins in antiferromagnets, are presently among the hottest topics in magnetism [7–9].

Recently, it was argued that nearly single-cycle terahertz (THz) pulses are the most energy efficient means of ultrafast spin control in antiferromagnets. Several reports demonstrated an efficient excitation of spins in antiferromagnetics NiO [10,11], TmFeO<sub>3</sub> [12–14], and FeBO<sub>3</sub> [15]. However, despite several attempts, no THz excitation and detection of coherent spin waves has been reported for hematite—the main component of rust, the most widespread mineral in nature, and, obviously, the most widespread antiferromagnet.

Here, we explore the efficiency of THz excitation of spins in antiferromagnetic  $\alpha$ -Fe<sub>2</sub>O<sub>3</sub>. We demonstrate experimentally and theoretically that the mechanism of spin excitation relies on a magnetic-dipole interaction of the THz magnetic field and spins and the efficiency of the coupling is proportional to the time derivative of the THz magnetic field.

The paper is organized as follows. Section II reports about details of the studied sample, its characterization, and experimental procedure. Section III describes the main experimental results. Section IV proposes a thermodynamic theory describing possible modes of spin resonance in this compound, the temperature dependencies of the modes, and the torques which can excite them. Based on a comparison of the theory with the experimental results, conclusions are drawn, which are summarized in the last section.

**II. EXPERIMENTAL PROCEDURE**

Hematite  $\alpha$ -Fe<sub>2</sub>O<sub>3</sub> is a prominent representative of a broad class of canted antiferromagnetic iron oxides. The Fe<sup>3+</sup> ions form two magnetic sublattices, the spins of which are antiferromagnetically (AF) coupled due to a symmetric exchange interaction. Similarly to FeBO<sub>3</sub>, the crystal structure of hematite  $\alpha$ -Fe<sub>2</sub>O<sub>3</sub> has the  $\bar{3}m$  point group [2,16].

\*k.grishunin@science.ru.nl; also at MIREA–Russian Technological University, Moscow 119454, Russia.

†Also at University of Cologne, Institute of Physics II, Cologne D-50937, Germany.

‡Deceased.

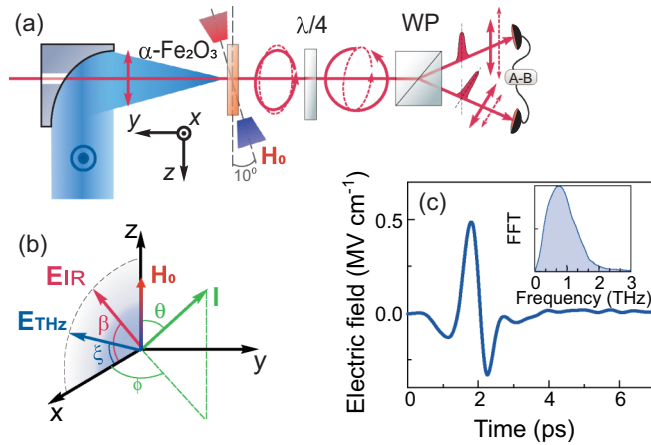


FIG. 1. Experimental geometry. (a) Experimental schematic for ultrafast terahertz (THz) pump-infrared (IR) probe spectroscopy. The corresponding polarization transformations of the IR pulse with and without a THz pump are shown by dashed and solid lines, respectively. (b) The corresponding schematic representation of the mutual orientations of antiferromagnetic vector  $\mathbf{l}$ , THz electric field ( $\mathbf{E}_{\text{THz}}$ ), the electric field of IR ( $\mathbf{E}_{\text{IR}}$ ) pulses, and the external magnetic field  $\mathbf{H}_0$ . (c) The incident THz electric field in a time domain and its Fourier transform (inset).

Below the Morin temperature ( $T < T_M = 260$  K), the magnetic moments are oriented along the [001] crystallographic axis and the material has no net magnetization. At  $T_M$  hematite undergoes a spin-flop phase transition. Above the Morin point, the direction of spins is parallel to the basal (001) plane with a slight in-plane canting. This canted or weak ferromagnetic (WF) phase persists up to the Néel temperature ( $T_N = 950$  K) above which the material becomes paramagnetic [17]. For the first time, the existence of the WF state was observed experimentally in hematite more than 60 years ago [17] and explained by Dzyaloshinskii [2] and Moriya [18] as a consequence of an antisymmetric exchange interaction between atomic spins. It should be also noted that near the Morin transition temperature the WF and AF phases may coexist [19].

In our studies we used a 500- $\mu\text{m}$ -thick plate of  $\alpha$ -hematite ( $\alpha\text{-Fe}_2\text{O}_3$ ) with a [001] crystallographic axis along the normal to the sample. The crystal was grown by the floating zone melting method under an oxygen pressure of 60 atm at 1670 K with a growth rate of 8 mm/h. The details of the crystal growth can be found elsewhere [20].

We excited  $\alpha\text{-Fe}_2\text{O}_3$  with intense nearly single-cycle terahertz pulses generated by tilted-pulse-front optical rectification [21] of near-infrared laser pulses from an amplified Ti:sapphire laser ( $\lambda = 800$  nm; pulse duration  $\Delta\tau = 100$  fs; the repetition rate is 1 kHz). The generated THz pulse beam was collimated and focused onto the sample by using off-axis parabolic mirrors [see Fig. 1(a)]. The focal lengths of the mirrors were chosen to provide the smallest spot diameter of about 500  $\mu\text{m}$  at full width at half maximum (FWHM). The polarization of the THz pulse was varied by using a combination of two wire-grid polarizers where the second polarizer set the output THz polarization direction, while the first ensured constant intensity onto the sample. The peak THz

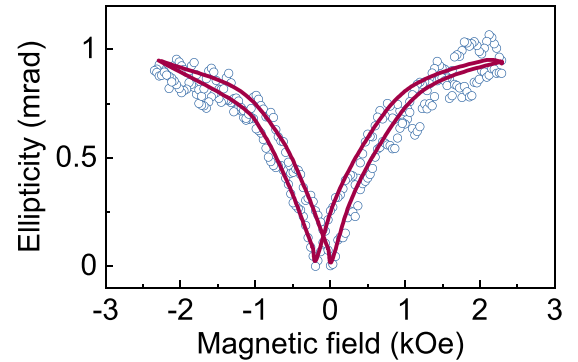


FIG. 2. Ellipticity acquired by linearly polarized light as a function of the external magnetic field at  $T = 293$  K. The solid line serves as a guide for the eye.

electric field was up to 0.5 MV/cm. The pulse spectrum range from 0.1 to 2 THz covers the characteristic frequency of the antiferromagnetic resonance [Fig. 1(c)]. The induced ultrafast spin dynamics is revealed by tracking the ellipticity of a copropagating 100-fs IR laser pulse generated by an optical parametric amplifier with a central wavelength  $\lambda = 1350$  nm in the transmission geometry. To ensure that after every pump pulse and relaxation the very same initial state of the medium is restored, an external magnetic field  $H_0 \approx 0.64$  kOe was applied at an angle of  $10^\circ$  to the sample plane.

Conventionally, the magnetic structure of weak ferromagnets is described by antiferromagnetic  $\mathbf{l} = (\mathbf{M}_1 - \mathbf{M}_2)/2M_0$  and ferromagnetic  $\mathbf{m} = (\mathbf{M}_1 + \mathbf{M}_2)/2M_0$  macrospin parameters, where  $\mathbf{M}_1$  and  $\mathbf{M}_2$  are the saturation magnetizations of the two antiferromagnetically coupled sublattices and  $M_0 = 870$  G is the saturation magnetization for each of the sublattices.

Figure 2 shows how the ellipticity acquired by linearly polarized probe light upon propagation through the sample depends on the applied magnetic field at room temperature. The dependence is even with respect to the applied external magnetic field. Hence the ellipticity must be explained as a result of magnetic contributions to the symmetric part of the dielectric permittivity tensor  $\epsilon_{ij}^{(s)} = \epsilon_{ji}^{(s)}$ .

### III. RESULTS

A time trace of the THz-induced dynamics contains oscillations with a frequency of 200 GHz at room temperature [Fig. 3(a)]. The frequency of the observed oscillations is in the ballpark of the one for the quasi-antiferromagnetic mode (q-AFM) in this compound. We performed the time-resolved measurements in a broad range of temperatures and processed the obtained time traces (see Fig. S1 in the Supplemental Material [22]) using the Fourier transform [see Fig. 3(b)]. It is seen that both the amplitude and the frequency of the oscillations change dramatically with temperature. Close to the temperature of the Morin transition, the frequency of the oscillations softens down to 82 GHz. With a further decrease of the temperature to 6 K, the frequency slowly increases and returns to 200 GHz [Fig. 3(c)]. This behavior is in qualitative agreement with the one expected for the q-AFM mode in the hematite [23–25].

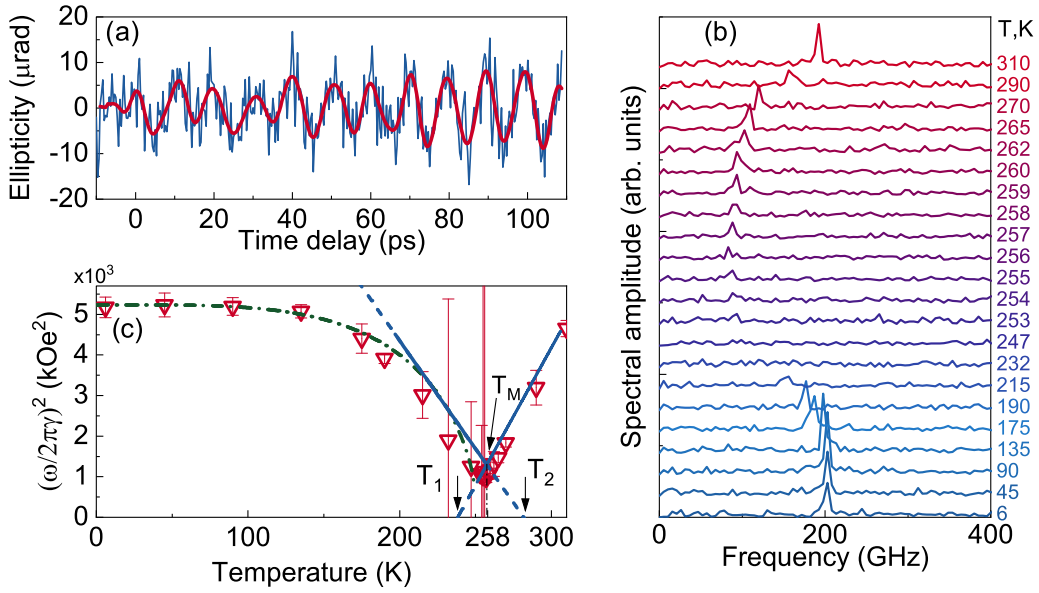


FIG. 3. Terahertz-induced magnetization dynamics in  $\alpha\text{-Fe}_2\text{O}_3$ . (a) Transient ellipticity of the IR probe pulse as a function of the time delay between the THz pump and IR probe pulse. The solid line is a filtered signal, serving as a guide for the eye. (b) The Fourier spectra of the transient ellipticity time traces measured at different temperatures. Corresponding time domain traces are shown in Fig. S1 in the Supplemental Material [22]. (c) Squared resonance frequencies of the q-AFM mode as a function of the sample temperature. Red triangles show the experimental data; blue lines show the fit with Eqs. (14) and (19); the green dashed-dotted line shows fit using the spin-wave model [24,26].

To reveal the mechanisms of excitation and detection of the mode, we systematically varied the orientation of the electric field of the THz pump  $\mathbf{E}_{\text{THz}}$  ( $\xi$ ) and infrared probe  $\mathbf{E}_{\text{IR}}$  ( $\beta$ ) pulses in the  $x$ - $z$  plane at  $T = 293$  K, i.e., above the Morin temperature. The observed time traces were processed with the help of the Fourier analysis and the corresponding dependencies of the Fourier amplitudes of the q-AFM mode are shown in Fig. 4.

The THz polarization dependence is unipolar and reaches maximum when the magnetic field of the THz pulse coincides with the direction of the external magnetic field  $\mathbf{H}_0$ . In other words, a nonzero response in the time domain is observed when the THz magnetic field is parallel to the net magnetization in the WF phase, i.e., nearly perpendicular to the slightly canted spins.

The probe polarization dependence shows two extrema at  $\beta \approx \pm 45^\circ$  and changes the sign in the vicinity of  $\beta = 0^\circ$ . Similar behavior was observed in the experiments with  $\text{FeBO}_3$  [15]. Such a dependence evidences that the polarization ellipticity detected in the measurements originates from the magneto-optical Cotton-Mouton effect.

However, if the detection mechanism in the WF phase seems to be clear, a much lower signal-to-noise ratio below  $T_M$  prevents us from experimental verification of the origin of the q-AFM mode in the AF phase. This is why we propose an extensive theoretical analysis of the problem.

#### IV. THEORETICAL ANALYSIS AND DISCUSSION

##### A. Detection mechanism

A light-matter interaction in the simplest case of the electric-dipole approximation is defined by the dielectric permittivity tensor  $\epsilon_{ik}$ . Neglecting dissipations in the crystal, it

can be shown that the tensor is Hermitian ( $\epsilon_{ji} = \epsilon_{ij}^*$ ) [27]. Expansion of the tensor in a power series of  $\mathbf{I}$  up to second-order terms and the subsequent diagonalization of the tensor show that light in such a crystal will have two mutually orthogonal modes with refractive indices  $n_{1,2}$ . In particular, for the case

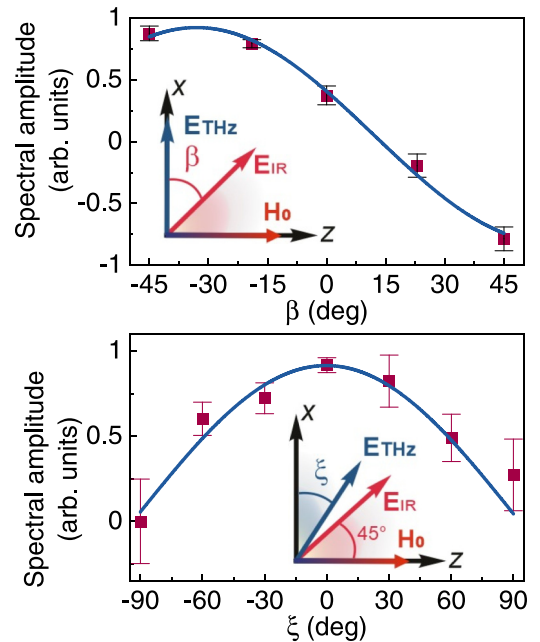


FIG. 4. The Fourier spectral amplitude of the q-AFM mode as a function of the polarization direction of the probe pulse  $\beta$  for  $\xi = 0^\circ$  (a) and of the pump pulse  $\xi$  for  $\beta = 45^\circ$  (b). The measurements were performed at  $T = 293$  K. The solid lines correspond to fits with functions given by Eqs. (16) and (3), respectively.

of a single domain ( $\mathbf{H}_{\text{ext}} \neq 0$ ) and  $\mathbf{k} \parallel c$  axis we obtain [28]

$$n_{1,2}^2 = \frac{1}{2} [(\Omega_{xx} + \Omega_{zz}) \pm \sqrt{(\Omega_{xx} - \Omega_{zz})^2 + 4\Omega_{zx}^2}], \quad (1)$$

where  $\Omega_{xx} = \epsilon_{xx} - \epsilon_{xy}^2/\epsilon_{yy}$ ,  $\Omega_{zz} = \epsilon_{zz} - \epsilon_{zy}^2/\epsilon_{yy}$ , and  $\Omega_{zx} = \epsilon_{zx} - \epsilon_{zy}\epsilon_{xy}^*/\epsilon_{yy}$ . We use Cartesian coordinates where the direction of the  $y$  axis coincides with the optical axis ([001] crystallographic axis), while the  $x$  and the  $z$  axes lie in the sample plane and  $x$  is parallel to the direction of the external magnetic field [Fig. 1(b)].

In the expansion of the dielectric tensor only the symmetric part  $\epsilon_{ij}^{(s)} = \epsilon_{ji}^{(s)}$  depends on the quadratic terms with respect to  $\mathbf{l}$ . This dependence eventually results in magnetic linear birefringence and magnetic linear dichroism, which are also often called the magneto-optical Cotton-Mouton effect [29].

In order to understand how the polarization of the IR pulse changes upon propagation, we use the formalism of the Jones matrices [30]. First, the electrical vector of the optical pulse is rotated from the laboratory coordinate system to the frame of the crystallographic axes. Subsequently, static phase retardation  $\Gamma$  in the sample is introduced and, finally, the electric vector is returned back to the laboratory coordinate system.

By applying a similar procedure we take into account the optical elements in our detection, consisting of a quarter-wave plate, Wollaston prism, and balanced detector. It can be shown that the signal in the differential channel of the balance detector can be written in the following form,

$$I_{D1-D2} \propto E_0^2 \sin(\Gamma) \sin(2\beta), \quad (2)$$

where  $E_0$  is the electric field of the IR pulse at the detector.

If the THz pulse is applied, the total phase retardation  $\Gamma$  can be represented as a sum of the time-independent and the THz-induced contributions  $\Gamma = \Gamma_0 + \delta\Gamma(t)$ . Taking into account that the THz-induced signal is relatively small compared to the static one  $\Gamma_0$ , we obtain

$$I_{D1-D2} \propto E_0^2 \sin(2\beta) \cos(\Gamma_0) \delta\Gamma(t). \quad (3)$$

Equation (3) shows how the detected signal depends on the retardation  $\delta\Gamma(t)$ . The latter is induced via the Cotton-Mouton effect when the Néel vector  $\mathbf{l}$  oscillates in the sample plane (WF,  $T > T_M$ ).

## B. Ground state

An equilibrium orientation of the magnetization is determined by the minimum of free energy of the crystal. The expansion of the thermodynamic potential, containing the invariants with respect to the  $\bar{3}m(D_{3d})$  point group of  $\alpha\text{-Fe}_2\text{O}_3$  in terms of normalized antiferromagnetic  $\mathbf{l}$  and ferromagnetic  $\mathbf{m}$  vectors, takes the following form [2,16,31]:

$$W = \frac{1}{2}\tilde{\mathcal{J}}\mathbf{m}^2 + \frac{1}{2}b_1(\mathbf{l} \cdot \mathbf{n})^2 + \frac{1}{4}b_2(\mathbf{l} \cdot \mathbf{n})^4 + \frac{1}{2}D(\mathbf{m} \cdot \mathbf{l})^2 - 2M_0\mathbf{m} \cdot \mathbf{H}_t, \quad (4)$$

Here,  $\tilde{\mathcal{J}} = 4H_{\text{ex}1}M_0$  and  $D = 4H_{\text{ex}2}M_0$  are the effective values describing the isotropic exchange interaction, and  $b_1 = 2H_{a1}M_0$  and  $b_2 = -2H_{a2}M_0$  are uniaxial out-of-plane anisotropy constants of the second and the fourth order, respectively.  $\mathbf{n}$  is the direction of the easy axis. The last term  $\mathbf{H}_t = \mathbf{H}_0 + \mathbf{H}_{\text{THz}} + \mathbf{d} \times \mathbf{l}$  comprises the interactions with the static external magnetic field  $\mathbf{H}_0$ , the magnetic field of the

THz pulse  $\mathbf{H}_{\text{THz}}$ , and the Dzyaloshinskii interaction, where the Dzyaloshinskii vector  $\mathbf{d}$  is oriented along the [001] crystallographic axis.

Looking for a minimum of the thermodynamic potential given by Eq. (4) and neglecting the longitudinal magnetic susceptibility  $\chi_{\parallel}$  of the antiferromagnet with respect to the transverse one  $\chi_{\perp} = 4M_0^2/\tilde{\mathcal{J}}$  ( $D\mathbf{l}^2 \gg \tilde{\mathcal{J}}$ ), one can represent  $\mathbf{m}$  as a function of  $\mathbf{l}$ ,

$$\mathbf{m} = \frac{\chi_{\perp}}{2M_0} [\mathbf{H}_t - \mathbf{l}(\mathbf{H}_t \cdot \mathbf{l})], \quad (5)$$

where we assumed that  $|\mathbf{M}_1| = |\mathbf{M}_2| = M_0$ . This is equivalent to  $\mathbf{m}^2 + \mathbf{l}^2 = 1$  and  $\mathbf{m}\mathbf{l} = 0$  [16].

Substituting (5) in (4) gives

$$W = \frac{1}{2}b_1(\mathbf{l}, \mathbf{n})^2 + \frac{1}{4}b_2(\mathbf{l}, \mathbf{n})^4 - \frac{\chi_{\perp}}{2} [\mathbf{H}_t^2 - (\mathbf{H}_t \cdot \mathbf{l})^2]. \quad (6)$$

The minimum depends on the mutual orientation of the vectors  $\mathbf{l}$  and  $\mathbf{n}$ . In order to define the magnetic ground state of the crystal, it is convenient to introduce the q-AFM vector in spherical coordinates:  $\mathbf{l} = (\sin \theta \cos \varphi, \sin \theta \sin \varphi, \cos \theta)$ . Then, the total energy (6) is given by the expression

$$W = \frac{1}{2}\tilde{b}_1 \sin^2 \theta \sin^2 \varphi + \frac{1}{4}b_2 \sin^4 \theta \sin^4 \varphi - \frac{\chi_{\perp}}{2} H_0^2 \sin^2 \theta, \quad (7)$$

where the Dzyaloshinskii field is included in the redefined single-ion anisotropy constant  $\tilde{b}_1 = b_1 - \chi_{\perp} \mathbf{d}^2$ .

There are two stable states for  $\theta$  and  $\varphi$  that satisfy the global minimum of free energy: WF or an easy plane (EP) and AF or an easy axis (EA). The EP phase corresponds to the case when  $\mathbf{l} \perp c$  while for the EA phase  $\mathbf{l} \parallel c$ .

Finding the minimum value of the potential (7), it is important to note that if  $\mathbf{H}_0^2 \ll \mathbf{d}^2$  and  $b_2 < 0$ , the stability regions for  $\mathbf{l} \parallel c$  and  $\mathbf{l} \perp c$  overlap. Indeed, since  $\tilde{b} = \tilde{b}(T)$ , the expansion of free energy in a Taylor series with powers of  $T - T_1$ , where  $T_1$  is the temperature at which the high-temperature phase loses stability, shows the coexistence of two different phases:

$$\mathbf{l} \perp c : \theta_0 = \frac{\pi}{2}, \quad \varphi = 0, \pi \quad \text{at } T > T_1, \quad (8)$$

$$\mathbf{l} \parallel c : \theta_0 = \frac{\pi}{2}, \quad \varphi = \frac{\pi}{2}, \frac{3\pi}{2} \quad \text{at } T < T_2 = T_1 \left(1 + \frac{|b_2|}{b}\right). \quad (9)$$

Estimates of the corresponding temperatures will be given below.

## C. Excitation mechanism

The oscillations and their temperature dependencies can be understood by starting out with the expressions for the effective Lagrangian  $\mathcal{L}$  and the dissipative Rayleigh function  $\mathcal{R}$  [32,33]. In the selected spherical coordinates they take the

following form:

$$\mathcal{L} = \frac{\chi_{\perp}}{2} \left[ \left( \frac{\dot{\varphi}}{\gamma} - H_z \right) \sin \theta + (H_x \cos \varphi + H_y \sin \varphi) \cos \theta \right]^2 + \frac{\chi_{\perp}}{2} \left( \frac{\dot{\theta}}{\gamma} - H_x \sin \varphi + H_y \cos \varphi \right)^2 - \frac{1}{2} b_1 \sin^2 \theta \sin^2 \varphi - \frac{1}{4} b_2 \sin^4 \theta \sin^4 \varphi, \quad (10)$$

$$\mathcal{R} = \frac{\alpha M_0}{\gamma} (\dot{\theta}^2 + \sin^2 \theta \dot{\varphi}^2), \quad (11)$$

where  $\gamma$  is the gyromagnetic ratio, and  $\alpha$  is the Gilbert damping constant. The  $H_x$ ,  $H_y$ ,  $H_z$  are the components of  $\mathbf{H}_t = (d \cos \theta, 0, H_0 - d \sin \theta \cos \varphi)$ .

Above the Morin point, i.e., in the WF easy-plane phase ( $T > T_M$ ), the linearized Lagrange-Euler equations  $\frac{d}{dt} \left( \frac{\partial \mathcal{L}}{\partial \dot{\theta}} \right) - \frac{\partial \mathcal{L}}{\partial \theta} + \frac{\partial \mathcal{R}}{\partial \theta} = 0$ , etc., with the angles  $\theta = \theta_1 + \pi/2$  and  $\varphi = \varphi_1 + 0$  take the following form:

$$\ddot{\theta}_1 + \frac{2}{\tau} \dot{\theta}_1 + \gamma^2 (H_0^2 - H_0 d) \theta_1 = 0, \quad (12)$$

$$\ddot{\varphi}_1 + \frac{2}{\tau} \dot{\varphi}_1 + \gamma^2 \left( d(d - H_0) + \frac{b_1}{\chi_{\perp}} \right) \varphi_1 = \gamma \dot{H}_z, \quad (13)$$

where  $\tau$  is a damping constant [33,34].

A characteristic property of the dynamic equations (12) and (13) is that the driving force is proportional to  $d\mathbf{H}/dt$ . This effect was first predicted theoretically in Refs. [33,34], and then later demonstrated in NiO [10,35].

If we identify  $H_D \equiv -d$ ,  $H_c^2 = 2H_{\text{ex1}}H_{\text{a1}}$ , and take into account that  $d(d - H_0) \approx d^2$ , we recover the well-known expressions for q-AFM and q-FM frequencies:

$$\omega_{\text{AFM}}^2 \approx \gamma^2 [H_c^2 + H_D(H_0 + H_D)], \quad (14)$$

$$\omega_{\text{FM}}^2 = \gamma^2 (H_0^2 + H_0 H_D). \quad (15)$$

It is seen that the equations of motion (12) and (13) have a form typical for a damped harmonic oscillator, where the magnetic-dipole (Zeeman) interaction between the spins and the magnetic field of the THz pulse acts as a torque for the q-AFM mode. Interestingly, in the geometry of the experiment the torque for the q-FM mode is equal to zero. A resonant excitation of the q-AFM mode with the THz magnetic field  $\mathbf{H}_{\text{THz}} = H_{\perp}(t)(-\sin \xi, 0, \cos \xi)$  gives

$$\varphi_1(t) = -\gamma H_{\perp}^{\omega_{\text{AFM}}} \cos(\omega_{\text{AFM}} t) e^{-t/\tau} \cos \xi. \quad (16)$$

This dependence of the orientation of the THz magnetic field is in good agreement with the experimental data in the WF ( $T > T_M$ ) phase [Fig. 4(b)].

The dependence of  $H_c^2$  is linear with respect to temperature  $H_c^2 = aT + p$ . Substituting the values for  $a = 0.067 \times 10^3$  kOe<sup>2</sup>/K,  $p = -16.7 \times 10^3$  kOe<sup>2</sup>, and  $H_D = 22$  kOe from Ref. [23], the fit with Eq. (14) shows very good agreement with the experimental data [Fig. 3(c), blue solid line].

Repeating the linearization procedure for the AF easy-axis phase ( $T < T_M$ ,  $\theta = \theta_1 + \pi/2$ , and  $\varphi = \varphi_1 + \pi/2$ ), we obtain

$$\ddot{\theta}_1 + \frac{2}{\tau} \dot{\theta}_1 - \frac{\gamma^2}{\chi_{\perp}} (b_1 + b_2 - 2\chi_{\perp} H_0^2) \theta_1 = \gamma \dot{H}_x, \quad (17)$$

$$\ddot{\varphi}_1 + \frac{2}{\tau} \dot{\varphi}_1 - \frac{\gamma^2}{\chi_{\perp}} (b_1 + b_2) \varphi_1 = \gamma \dot{H}_z. \quad (18)$$

Returning to the definitions of the exchange and the anisotropy fields and neglecting the external magnetic field

with respect to the anisotropy field, we observe the case of two degenerate modes of antiferromagnetic resonance with the frequency:

$$\omega_{\text{AFM}}^2 = \gamma^2 H_{\text{ex1}} (H_{\text{a2}} - H_{\text{a1}}). \quad (19)$$

As in the previous case, the equations of motion are equations for harmonically damped oscillators and the q-AFM mode can be triggered with the Zeeman torque. Thereby, the solution is as follows:

$$\begin{pmatrix} \theta_1(t) \\ \varphi_1(t) \end{pmatrix} = -\gamma H_{\perp}^{\omega_{\text{AFM}}} \cos(\omega_i t) e^{-t/\tau} \begin{pmatrix} -\sin \xi \\ \cos \xi \end{pmatrix}, \quad (20)$$

where  $H_{\perp}^{\omega_{\text{AFM}}}$  is the spectral component of the magnetic field of the THz pulse at the frequency of the AFM mode  $\omega$  in the AF easy-axis phase.

The fit of the temperature dependence below the Morin temperature ( $T < T_M$ ) using Eq. (19) shows good agreement with the experimental data in the vicinity of  $T_M$  (Fig. 3, blue solid line).

An extension of the theory to the low-temperature range can be obtained with the help of a spin-wave model [24,26]. The fit with this model is shown as a green dashed-dotted line in Fig. 3(c). However, despite the good match one should remember that the spin-wave model simply has more fit parameters.

Finally, we can estimate the values for the temperatures  $T_1$  and  $T_2$  at which the WF and the AF phases lose stability. The temperatures  $T_1$  and  $T_2$  can be obtained by extrapolation of the temperature dependence of the frequency of the q-AFM mode given by Eqs. (14) and (19) to the intersections with the horizontal axis [see Fig. 3(c)]. The intersection of the two lines gives the value of the Morin temperature  $T_M$ . At this point the WF and AF phases have equal free energies. Thus, substituting the values  $b_1 = 200$  Oe and  $b_2/b_1 = -0.23$  [36], from Eqs. (14) and (19) we obtain the following estimates:  $T_1 \approx 235$  K,  $T_2 \approx 282$  K,  $T_M \approx 258$  K. The obtained Morin transition temperature is close to the values reported earlier [2,17,23].

## V. CONCLUSIONS

We experimentally demonstrated that ultrafast dynamics triggered in hematite  $\alpha$ -Fe<sub>2</sub>O<sub>3</sub> by intense nearly single-cycle terahertz pulses. We show that the dynamics corresponds to the quasi-antiferromagnetic resonant mode in the compound. The mode is detected due to the magneto-optical Cotton-Mouton effect and excited via the mechanism of a magnetic dipole interaction of a THz magnetic field with spins. The coupling efficiency is proportional to the time derivative of the magnetic field of the THz pulse and reaches

the maximum when the orientation of the THz magnetic field is perpendicular to the antiferromagnetically coupled spins. Using theoretically derived expressions we fitted the experimentally observed temperature dependencies of the mode near the Morin point and estimated the temperatures at which the high- and low-temperature phases lose stability.

## ACKNOWLEDGMENTS

The authors thank S. Semin and C. Berkhout for technical support. This work was supported by de Nederlandse Organisatie voor Wetenschappelijk Onderzoek (NWO) and the Russian Foundation for Basic Research (Grant No. 18-02-40027).

- [1] L. Néel, Propriétés magnétiques des ferrites; ferrimagnétisme et antiferromagnétisme, *Ann. Phys.* **12**, 137 (1948).
- [2] I. Dzyaloshinsky, A thermodynamic theory of “weak” ferromagnetism of antiferromagnetics, *J. Phys. Chem. Solids* **4**, 241 (1958).
- [3] S. Piramanayagam and T. C. Chong, *Developments in Data Storage: Materials Perspective* (Wiley, Hoboken, NJ, 2011), p. 352.
- [4] E. V. Gomonay and V. M. Loktev, Spintronics of antiferromagnetic systems, *Low Temp. Phys.* **40**, 17 (2014).
- [5] K. Olejník, T. Seifert, Z. Kašpar, V. Novák, P. Wadley, R. P. Campion, M. Baumgartner, P. Gambardella, P. Němec, J. Wunderlich, J. Sinova, P. Kužel, M. Müller, T. Kampfrath, and T. Jungwirth, Terahertz electrical writing speed in an antiferromagnetic memory, *Sci. Adv.* **4**, eaar3566 (2018).
- [6] N. Thielemann-Kühn, D. Schick, N. Pontius, C. Trabant, R. Mitzner, K. Holldack, H. Zabel, A. Föhlisch, and C. Schüßler-Langeheine, Ultrafast and Energy-Efficient Quenching of Spin Order: Antiferromagnetism Beats Ferromagnetism, *Phys. Rev. Lett.* **119**, 197202 (2017).
- [7] T. Jungwirth, X. Marti, P. Wadley, and J. Wunderlich, Antiferromagnetic spintronics, *Nat. Nanotechnol.* **11**, 231 (2016).
- [8] R. Lebrun, A. Ross, O. Gomonay, V. Baltz, U. Ebels, A.-L. Barra, A. Qaiumzadeh, A. Brataas, J. Sinova, and M. Kläui, Long-distance spin-transport across the Morin phase transition up to room temperature in ultra-low damping single crystals of the antiferromagnet  $\alpha$ -Fe<sub>2</sub>O<sub>3</sub>, *Nat. Commun.* **11**, 6332 (2020).
- [9] V. Baltz, A. Manchon, M. Tsoi, T. Moriyama, T. Ono, and Y. Tserkovnyak, Antiferromagnetic spintronics, *Rev. Mod. Phys.* **90**, 015005 (2018).
- [10] T. Kampfrath, A. Sell, G. Klatt, A. Pashkin, S. Mährlein, T. Dekorsy, M. Wolf, M. Fiebig, A. Leitenstorfer, and R. Huber, Coherent terahertz control of antiferromagnetic spin waves, *Nat. Photonics* **5**, 31 (2011).
- [11] S. Baierl, J. H. Mentink, M. Hohenleutner, L. Braun, T.-M. Do, C. Lange, A. Sell, M. Fiebig, G. Woltersdorf, T. Kampfrath, and R. Huber, Terahertz-Driven Nonlinear Spin Response of Antiferromagnetic Nickel Oxide, *Phys. Rev. Lett.* **117**, 197201 (2016).
- [12] S. Baierl, M. Hohenleutner, T. Kampfrath, A. K. Zvezdin, A. V. Kimel, R. Huber, and R. V. Mikhaylovskiy, Nonlinear spin control by terahertz-driven anisotropy fields, *Nat. Photonics* **10**, 715 (2016).
- [13] K. Grishunin, T. Huisman, G. Li, E. Mishina, T. Rasing, A. V. Kimel, K. Zhang, Z. Jin, S. Cao, W. Ren, G.-H. Ma, and R. V. Mikhaylovskiy, Terahertz magnon-polaritons in TmFeO<sub>3</sub>, *ACS Photonics* **5**, 1375 (2018).
- [14] S. Schlauderer, C. Lange, S. Baierl, T. Ebnet, C. P. Schmid, D. C. Valovcin, A. K. Zvezdin, A. V. Kimel, R. V. Mikhaylovskiy, and R. Huber, Temporal and spectral fingerprints of ultrafast all-coherent spin switching, *Nature (London)* **569**, 383 (2019).
- [15] E. A. Mashkovich, K. A. Grishunin, R. V. Mikhaylovskiy, A. K. Zvezdin, R. V. Pisarev, M. B. Strugatsky, P. C. M. Christianen, T. Rasing, and A. V. Kimel, Terahertz Optomagnetism: Nonlinear THz Excitation of GHz Spin Waves in Antiferromagnetic FeBO<sub>3</sub>, *Phys. Rev. Lett.* **123**, 157202 (2019).
- [16] E. Turov, in *Physical Properties of Magnetically Ordered Crystals*, edited by A. Tybulewicz (Academic, New York, 1965), p. 222.
- [17] F. J. Morin, Magnetic susceptibility of  $\alpha$ -Fe<sub>2</sub>O<sub>3</sub> and  $\alpha$ -Fe<sub>2</sub>O<sub>3</sub> with added titanium, *Phys. Rev.* **78**, 819 (1950).
- [18] T. Moriya, Anisotropic superexchange interaction and weak ferromagnetism, *Phys. Rev.* **120**, 91 (1960).
- [19] M.-Z. Dang, D. Rancourt, J. Dutrizac, G. Lamarche, and R. Provencher, Interplay of surface conditions, particle size, stoichiometry, cell parameters, and magnetism in synthetic hematite-like materials, *Hyperfine Interact.* **117**, 271 (1998).
- [20] A. M. Balbashov, Contemporary apparatus for single crystals growth of oxide compounds and metals by optical floating zone (FZ), *Crystals* **9**, 487 (2019).
- [21] J. Hebling, G. Almasi, I. Kozma, and J. Kuhl, Velocity matching by pulse front tilting for large area THz-pulse generation, *Opt. Express* **10**, 1161 (2002).
- [22] See Supplemental Material at <http://link.aps.org/supplemental/10.1103/PhysRevB.104.024419> for the dependencies of ellipticity of the IR pulse as a function of the time delay between THz pump and IR probe pulses at different temperatures.
- [23] L. Velikov and E. Rudashevskii, Antiferromagnetic resonance in hematite in the weakly ferromagnetic state, *JETP Lett.* **29**, 836 (1969).
- [24] S. G. Chou, P. E. Stutzman, S. Wang, E. J. Garboczi, W. F. Egelhoff, and D. F. Plusquellic, High-Resolution Terahertz optical absorption study of the antiferromagnetic resonance transition in hematite ( $\alpha$ -Fe<sub>2</sub>O<sub>3</sub>), *J. Phys. Chem. C* **116**, 16161 (2012).
- [25] R. Mikhaylovskiy, E. Hendry, A. Secchi, J. Mentink, M. Eckstein, A. Wu, R. Pisarev, V. Kruglyak, M. Katsnelson, T. Rasing, and A. Kimel, Ultrafast optical modification of exchange interactions in iron oxides, *Nat. Commun.* **6**, 8190 (2015).
- [26] O. Nagai, N. L. Bonavito, and T. Tanaka, On the magnon interaction in haematite. II. Magnon energy of acoustical mode and magnetic critical fields, *J. Phys. C* **8**, 176 (1975).
- [27] L. Landau and E. Lifshitz, *Electrodynamics of Continuous Media*, Course of Theoretical Physics Vol. 8 (Pergamon, Oxford, UK, 1984), p. 460.
- [28] I. S. Akhmadullin, V. A. Golenishchev-Kutuzov, S. A. Migachev, and M. F. Sadykov, Magnetic birefringence of light in hematite, *Phys. Solid State* **44**, 333 (2002).

- [29] J. Ferre and G. A. Gehring, Linear optical birefringence of magnetic crystals, *Rep. Prog. Phys.* **47**, 513 (1984).
- [30] R. Azzam and N. Bashara, *Ellipsometry and Polarized Light* (Elsevier–North-Holland, Amsterdam, 1977), p. 548.
- [31] M. B. Strugatsky and K. M. Skibinsky, Effective hexagonal magnetic anisotropy of hematite: Accounting for higher-order invariants, *Phys. Solid State* **57**, 1524 (2015).
- [32] A. F. Andreev and V. I. Marchenko, Symmetry and the macroscopic dynamics of magnetic materials, *Sov. Phys. Usp.* **23**, 21 (1980).
- [33] A. K. Zvezdin and A. A. Mukhin, New nonlinear dynamics effects in antiferromagnets, *Kratkie Soobshcheniya po Fizike FIAN* **12**, 10 (1981) [Soviet Physics - Lebedev Institute Reports].
- [34] A. Zvezdin, Dynamics of domain walls in weak ferromagnets, *JETP Lett.* **29**, 553 (1979).
- [35] T. Satoh, S.-J. Cho, R. Iida, T. Shimura, K. Kuroda, H. Ueda, Y. Ueda, B. A. Ivanov, F. Nori, and M. Fiebig, Spin Oscillations in Antiferromagnetic NiO Triggered by Circularly Polarized Light, *Phys. Rev. Lett.* **105**, 077402 (2010).
- [36] R. Levitin and V. Shchurov, Influence of the second uniaxial anisotropy constant on the magnetization curve of a uniaxial antiferromagnet with weak ferromagnetism, *JETP Lett.* **7**, 110 (1968).